IEEE Access
Multidisciplinary | Rapid Review | Open Access Journal

Received April 23, 2020, accepted May 7, 2020, date of publication May 12, 2020, date of current version May 28, 2020.

Digital Object Identifier 10.1109/ACCESS.2020.2994139

Fault Detection Based on the Generalized S-Transform With a Variable Factor for Resonant Grounding Distribution Networks

ZHINONG WEI, (Member, IEEE), YUEXUAN MAO, ZHIHUA YIN, GUOQIANG SUN, AND HAIXIANG ZANG

College of Energy and Electrical Engineering, Hohai University, Nanjing 210098, China

Corresponding author: Zhinong Wei (wzn_nj@263.net)

This work was supported by the Science and Technology Project of State Grid Jiangsu Electric Power Corporation through the Research and Demonstration of Efficient Fault Location Technology for Distribution Network Based on Multi-source Information under Grant J2017143-2.

ABSTRACT Fault detection in resonant grounding (RG) distribution networks remains a challenge due to weak fault signals, extremely complex fault conditions, and unstable intermittent arc grounding faults. This paper addresses this issue by applying generalized S-transform (GST) with a variable factor to conduct denoising of transient zero-sequence currents based on threshold filtering followed by time-frequency distribution filtering in sequence. Meanwhile, this paper proposes a comprehensive multi-criteria faulty feeder detection method based on the transient zero-sequence current polarity (criterion 1), the energy relative entropy (criterion 2), and the total transient current energy (criterion 3). Here, criteria 2 and 3 are based on the time-frequency representation of the GST. The performances of the proposed denoising and faulty feeder detection methods are evaluated under single line to ground faults based on simulations conducted using a modeled 10 kV RG networks with overhead and cable mixed lines in addition to reasonably sophisticated permanent and intermittent arc discharge models to ensure that the simulations faithfully represent actual complex working conditions. Compared with existing method, simulation experiments and field test show that the method proposed in this paper provide a better denoising effect with stronger self-adaptability, higher detection accuracy, and a faster calculation speed.

INDEX TERMS Fault detection, resonant grounding distribution networks, generalized S-transform, variable factor, denoising method, intermittent arc grounding fault, multi-criteria.

I. INTRODUCTION

Most of the distribution networks in China operating in the range of 10–35 kV are grounded by arc suppression coils. Such systems are typically denoted as resonant grounding (RG) distribution networks. Approximately 80% of faults that occur in RG networks are single line to ground (SLG) faults. Such faults are particularly serious because they can damage feeder insulation, and thereby lead to multi-point grounding that can critically detract from system stability and power supply reliability. The seriousness of SLG faults is indicated by the newest technical guidelines for distribution networks published in 2016 [1] instructing operators to identify faulty feeders as soon as possible after an SLG fault occurs, which represents a substantial upgrade in concern from the previous instruction to ''continue operating for 2 hours''. However, the detection of SLG faults in RG networks remains a challenge due to fault signals that are too weak to identify, frequent intermittent arc grounding faults with unstable signals, and complex working conditions such as noisy environments due to extensive cabling and limitations in measurement accuracy, and high impedance faults [2]–[5]. Hence, selecting the faulty feeder quickly and correctly is essential for ensuring the stability and reliability of RG networks.

A. PREVIOUS RELATED WORK

At present, the faulty feeder detection methods can be divided into two categories according to the origin of signals, which are the active detection [6] and the passive

The associate editor coordinating the review of this manuscript and approving it for publication was Francesco Tedesco.

TABLE 1. Pros and cons of the existing methods and the proposed method.

Signal processing method	Pros	Cons
WT	(i) A multi-resolution analysis that owns a time-frequency window that varies according to the frequency. (ii) Good time-frequency local property.	(i) Highly sensitive to noise and harmonics. (ii) More computational requirements with high sampling rate. (iii) The wavelet basis function is difficult to select which seriously restricts the adaptability of WT signal decomposition to accommodate variations in signal features.
HHT	(i) Applicable for the analysis of nonlinear and non-stationary signals. (ii) Requires no initial assumption of the signal and predetermined set of mathematical functions.	(i) End effect of empirical mode decomposition (EMD). (ii) The EMD mode mixing problem. (iii) The residual noise.
ST	(i) A lossless and reversible multiresolution time-frequency analysis method. (ii) Obtains amplitudes and phase angles of signals according to time and frequency.	(i) The specific mother wavelet renders adjustments to the time-frequency resolution inflexibly.
Prony algorithm	(i) A method for fitting data sampled in equal intervals using a linear combination of a set of exponential terms which overcomes the influence of asymmetric component and power frequency components. (ii) Immune to the influence of arc suppression coil.	(i) Fitting effect for high frequency signals is not good. (ii) Expensive computing cost and low speed of calculation. (iii) Susceptible to noise.
MM	(i) Precisely extracts apart from any distortions with reduced size of data window in real-time.	(i) Actual signal cannot be extracted under complex conditions including strong noise corruption and the unbalance system.
FCM	(i) Unsupervised pattern recognition. (ii) Simple procedures.	(i) Dependence on the quality of initialization data strongly. (ii) Easy to fall into local saddle point.
SVM	(i) Can be used for linear and nonlinear classification or regression. (ii) Low generalization error rate. (iii) Avoids neural network structure selection and local minima.	(i) Requires vast sample libraries. (ii) Complicated procedures. (iii) Long calculation times.
GST in this paper	(i) The GST is modified to include a variable factor for self-adaptively adjusting the local window resolution of the time-frequency spectrum. (ii) Can obtain the time-frequency matrix of a transient zero-sequence current signal. (iii) Good performance of signal denoising. (iv) Multi-resolution time-frequency analysis for linear and nonlinear signals.	(i) Although high computational complexity, the proposed method has a faster judgment speed with high accuracy. (ii) Complicated but comprehensive procedures.

detection. Owing to the richness and stability of transient fault signal features, the detection methods employed in RG systems are mainly the passive detection based on transient signals. Primary examples of detection methods employing these features include the wavelet transform (WT) [7]–[10], Hibert-Huang transform (HHT) [11], [12], S-transform (ST) [13]–[18], Prony algorithm [19], [20], mathematical morphology (MM) [21]–[23], fuzzy c-means (FCM) clustering [24], [25], and support vector machine (SVM) [26], [27]. Each of these techniques have pros and cons as listed in Table 1.

The WT provides a time-frequency window that varies according to the frequency so that it can extract time and frequency information from transient fault signals. Wang *et al.* [7] constructed a mixed atom dictionary by a cosine packet and a wavelet and adopted the matching pursuit algorithm to extract characteristic atoms of each feeder to extract transient signals. Guo *et al.* [8] used wavelet packet to make five-layer decomposition of main loop current firstly, and then, selected the effective coefficients based on the change rate of a wavelet packet energy entropy to reconstruct an effective signal of the arc fault. Guo *et al.* [9] acquired time-frequency gray scale images for all feeders via the continuous wavelet transform (CWT), and distinguished images associated with the faulty feeder from those associated with healthy feeders using a trained convolutional neural network (CNN). Fault detection has also been facilitated by applying the wavelet packet transform to segregate the high-frequency components of three-phase current signals during power swings [10].

The HHT employs empirical mode decomposition (EMD) and Hilbert transform, and is applicable for the analysis of nonlinear and non-stationary signals. Chen *et al.* [11] used the EMD to resolve the current into several intrinsic mode function (IMF), and then calculated Hilbert transform for IMF to obtain the Hilbert spectrum of arc fault current signals to recognize the series arc fault. Wang *et al.* [12] utilized complete ensemble EMD with adaptive noise (CEEMDAN) to extract

the first intrinsic mode function (IMF) of the zero-sequence current and used the Hilbert transform to obtain a fault detection index for identifying the faulty feeder.

For the ST, Stockwell *et al.* [13] presented a lossless and reversible multiresolution time-frequency analysis method in 1996, where the resolution was adjustable according to changes in the frequency based on a moving and scalable localizing Gaussian window. Pinnegar and Mansinha [14] modified the ST into a generalized ST (GST) form to obtain time-frequency spectra with different time-frequency resolutions by manually changing the value of an adjustable parameter. However, the process was not adaptive. Zhou and Chen [15] addressed this limitation in the local window resolution of the time-frequency spectrum by adopting a variable factor that improves the scalability of the localizing Gaussian window. He *et al.* [16] obtained the time-frequency matrix of transient zero-sequence currents via the GST, and realized fault section location by comparisons of the relative entropy of the transient current energies (i.e., transient current energy relative entropy). Fault detection has also been facilitated by extracting features from three-phase current signals by the ST, and distinguishing features associated with the faulty feeder from those associated with healthy feeders using a feedforward neural network (FFNN) [17]. Peng *et al.* [18] utilized ST to extract the standard amplitude ratios of the frequency components in zero-mode transients of each feeder and proposed a faulty feeder detection criterion by utilizing the amplitude information of the zero-mode transients captured at both terminals.

The Prony algorithm is a method for fitting data sampled in equal intervals using a linear combination of a set of exponential terms. Faulty feeder detection was conducted based on a linear relationship between the fault location and the inverse of the damping coefficient of the fundamental frequency component in the Prony model [19]. Liu *et al.* [20] utilized Prony algorithm to extract the transient information of main frequency components at each feeder to select faulty feeder.

The MM approach is a mature method of nonlinear signal analysis that was originally applied in the field of image signal processing. Barik *et al.* [21] was the first to utilize MM for identifying faulty feeders in RG systems. Shu *et al.* [22] detected faulty feeders according to the morphological peak-valley features of the constructed wavelet coefficients under characteristic bands. The morphological median filter is exploited to wrest unique fault features which are then fed as an input to a decision tree classifier to classify the fault type [23].

The FCM clustering algorithm automatically classifies sample data to obtain the membership of each sample point to sample centers. Guo and Yang [24] applied FCM clustering to the amplitude-polarity feature matrix (APFM) of transient fault signals to detect faulty feeders according to matrix elements lying outside of a threshold setting. Amplitude correlation coefficient matrix (ACCM) of transient zero-sequence currents was obtained via improved dynamic time warping (DTW), and then the faulty feeder was selected by FCM cluster method without setting threshold [25].

The SVM is a supervised learning model that serves as a kind of generalized linear classifier for the binary classification of data. An SVM classification algorithm has been employed for single-phase arc-fault detection in distribution networks based on a combination of transient zero-sequence current and two-phase current difference characteristics [26]. Chaitanya *et al.* [27] presented an high-impedance faults detection technique for distribution lines incorporating the distributed generators, where variational mode decomposition was used to obtain the analytic signal and then used this data as the input into the support vector machine to create an intelligent classifier.

B. PROBLEMS OF EXISTING FAULTY FEEDER DETECTION METHODS FOR RG SYSTEMS

1) FAULT SIGNAL PROCESSING

The presence of noise distorts the characteristics of fault signals. However, most existing methods extract fault features directly without first filtering the signals to remove noise.

2) FAULT FEATURE EXTRACTION

For WT-based methods, the wavelet basis function is difficult to select, and this seriously restricts the adaptability of WT signal decomposition to accommodate variations in signal features. The HHT has three problems that distort the signal decomposition results. These include the end effect of EMD, the EMD mode mixing problem, and the residual noise. The specific mother wavelet of the original ST proposed by Stockwell renders adjustments to the time-frequency resolution inflexibly because of the fixed window width of Gaussian window function, and the later proposed modifications to the GST are not effectively applied in fault detection. Signal feature extraction conducted by the Prony algorithm is susceptible to noise, and its fitting effect for high frequency signals is not good.

3) FAULTY FEEDER DETECTION CRITERIA

Most existing faulty feeder detection methods apply a single detection criterion. As a result, these methods are prone to incorrectly detect faulty feeders due to variations in signal features. Although multi-criteria methods have been developed to improve the accuracy of faulty feeder detection, existing methods are difficult to utilize because of the vast sample libraries required, complicated procedures, and long calculation times.

C. CONTRIBUTIONS

The above problems are addressed in the present study, and thereby makes the following contributions.

1) THE PURITY OF RECORDED FAULT DATA

The GST is modified to include a variable factor σ for self-adaptively adjusting the local window resolution of the

time-frequency spectrum, rather than simply narrowing the window with increasing frequency. Then, the modified GST, denoted as GST_σ, is employed to obtain the time-frequency matrix of a transient zero-sequence current signal. Denoising is then applied to the time-frequency matrix, and is conducted using a sequence of threshold filtering followed by time-frequency distribution filtering, which has been demonstrated to provide accurate denoising [28]. Most existing methods detect faulty feeder by recorded fault data without denoising, but this proposed method applies threshold filtering and time-frequency distribution filtering based on the generalized S-transform with a variable factor, which can detect correct faulty feeder in most noisy environments.

2) THE RELIABILITY OF MULTI-CRITERIA

A comprehensive multi-criteria faulty feeder detection method is established. Compared with existing single-criterion detection method, this proposed method includes three criteria (transient zero-sequence current polarity, transient current energy relative entropy, and total transient current energy) to reduce misjudgment. The second and third criteria are based on the time-frequency representation of the GST_σ approach. The method considers both the direction and energy of transient signal currents, which provides more comprehensive and accurate detection results than single-criterion methods. Meanwhile, the method is immune to overcompensation degrees, fault locations, fault resistances, initial fault angles, and noise intensities.

3) THE REALITY OF SIMULATION SYSTEM

The performances of the proposed denoising and faulty feeder detection methods are evaluated under both constant resistance faults and arc grounding faults based on simulations conducted using a modeled 10 kV RG distribution network with an overhead and cable mixed line structure in addition to a reasonably sophisticated arc discharge model to ensure that the simulations faithfully represent actual complex working conditions.

The proposed method is verified to provide a better denoising performance with stronger self-adaptability, higher detection accuracy, and a faster calculation speed compared with existing methods.

II. ANALYSIS OF TRANSIENT ZERO-SEQUENCE CURRENTS

An equivalent circuit of a transient SLG fault process in an RG system is illustrated schematically in Fig. 1, where C_0 is three-phase equivalent capacitance to ground, R_0 and L_0 are the respective equivalent resistance and inductance of the three-phase lines and all components in the zero-sequence circuit, L and r_L are the respective inductance and resistance of the arc suppression coil, u_0 is the equivalent zero-sequence supply voltage at the bus bar, i_d is the transient ground current, and i_L and i_C are the transient inductance and capacitance ground currents respectively produced by the arc suppression coil.

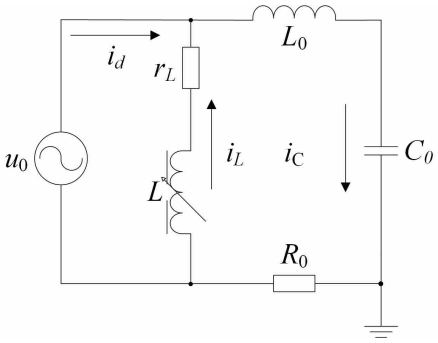

FIGURE 1. Equivalent circuit model of a transient single line to ground (SLG) fault process in a resonant grounding (RG) system.

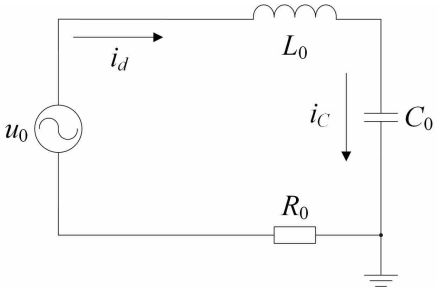

FIGURE 2. Equivalent circuit for a transient process without an arc suppression coil.

When an SLG fault occurs in an RG system, i_C is larger in magnitude and changes faster than i_L, which can therefore be ignored. As a result, $i_d = i_C$. Therefore, only transient capacitance currents are considered in this paper.

According to the simplified equivalent circuit presented in Fig. 2, i_C can be obtained as follows.

$$R_0 i_C(t) + L_0 \frac{di_C(t)}{dt} + \frac{1}{C_0}\int_0^t i_C(t)\,dt = U_m \sin(\omega t + \varphi) \quad (1)$$

Here, t is time, U_m is the voltage amplitude of the m-th phase, ω is the angular frequency of the steady-state power frequency components, and φ is its phase angle. In addition, we can define the amplitude of i_C as follows.

$$I_{Cm} = U_m \omega C_0, \quad t = 0 \quad (2)$$

The transient capacitance current $i_C(t)$ consists of the transient free oscillation component $i'_C(t)$ and the steady-state power frequency component $i''_C(t)$, which adhere to the following relationship.

$$i'_C(t) + i''_C(t) = 0, \quad t = 0 \quad (3)$$

According to (2) and (3), we can obtain the following equation by applying the Laplace transform.

$$\begin{cases} i_C(t) = i'_C(t) + i''_C(t) \\ i'_C(t) = I_{Cm}\left(\dfrac{\omega_f}{\omega} sin\varphi sin\omega_f t - cos\varphi cos\omega_f t\right) e^{-\delta t} \\ i''_C(t) = I_{Cm}\cos(\omega t + \varphi) \end{cases} \quad (4)$$

Here, ω_f and δ are the angular frequency and the attenuation coefficient of $i'_C(t)$, respectively, where $\delta = 1/\tau_C =$

$R_0/(2L_0)$, with τ_C represents a time constant. Therefore, when $\varphi = \pi/2$, the transient zero-sequence current can be calculated as follows.

$$i_0(t) = I_{Cm}\left(\frac{\omega_f}{\omega}e^{-\delta t}\sin\omega_f t - sin\omega t\right) \tag{5}$$

For a three-phase line, the grounding current $i_k(t)$ is three times greater than $i_0(t)$, which yields the following expression.

$$i_k(t) = 3I_{Cm}\left(\frac{\omega_f}{\omega}e^{-\delta t}\sin\omega_f t - sin\omega t\right) \tag{6}$$

Meanwhile, when an SLG fault occurs, the transient zero-sequence currents of the feeder lines adhere to the following characteristics in the selected frequency band (SFB) [29], [30].

(i) The amplitude of $i_C(t)$ is larger for a faulty feeder than that of any healthy feeder.

(ii) The flow direction of $i_C(t)$ (i.e., its polarity) is different for a faulty feeder than that for a healthy feeder, where $i_C(t)$ flows from the line to the bus bar for a faulty feeder, while $i_C(t)$ flows from the bus to the line for a healthy feeder.

III. DENOISING BASED ON THE MODIFIED GST

A. MODIFIED GST

As discussed above, Zhou and Chen [15] improved the scalability of the localizing Gaussian window used to define the local window resolution in GST by applying a variable factor σ_f, as follows.

$$\omega(t,f) = \frac{|f|}{\sigma_f\sqrt{2\pi}}e^{-\frac{t^2f^2}{e}}e^{-2\pi ft} \tag{7}$$

Here, f is the frequency and σ_f is dependent on the value of f, such as $\sigma_f(f) = af + b$, $\sigma_f(f) = a/f + b$, $\sigma_f(f) = (af + b)^\gamma$, where a, b, and γ are constants. For the linear variation $\sigma_f(f) = af + b$, the GST of a signal $h(t)$ is given as follows.

$$\mathrm{GST}_\sigma(\tau,f) = \int_{-\infty}^{+\infty} h(t)\frac{|f|}{(af+b)\sqrt{2\pi}}e^{-\frac{(\tau-t)^2f^2}{2(af+b)^2}}e^{-2\pi ft}dt \tag{8}$$

When $h[mT]$, $m = 0, 1, \ldots, N-1$ denote a discrete time series corresponding to $h(t)$ with a time sampling interval of T. The discrete Fourier transform is given as follows.

$$H\left[\frac{n}{NT}\right] = \frac{1}{N}\sum_{m=0}^{N-1}h[mT]\,e^{-\frac{i2\pi nm}{N}} \tag{9}$$

Here, $n = 0, 1, \ldots, N-1$. Equation (8) can be discretized by letting $f \to n/NT$ and $\tau \to kT$, where N is the number of sampling points, $n = 0, 1, 2, \ldots, N-1$ denotes the frequency sequence, $k = 0, 1, 2, \ldots, N-1$ denotes the time sequence, and T is the sampling interval, which yields the following discrete GST.

$$\mathrm{GST}_\sigma\left[kT, \frac{n}{NT}\right] = \sum_{m=0}^{N-1}H\left[\frac{n+m}{NT}\right]e^{\frac{-2\pi^2m^2{\sigma_f}^2}{n^2}}e^{\frac{i2\pi mn}{N}} \tag{10}$$

And for the $n = 0$ voice, the discrete GST can be defined as follows.

$$\mathrm{GST}_\sigma[kT, 0] = \frac{1}{N}\sum_{m=0}^{N-1}h\left(\frac{m}{NT}\right), \quad n = 0 \tag{11}$$

In the discrete signal analysis, the maximum frequency is denoted as $f_{\max}$ and σ_f is given as

$$\sigma_f = \alpha + \frac{\beta f}{f_{\max}}, \tag{12}$$

where $\alpha = 0.3$, $\beta = 8$, and σ_f is a monotonically increasing function of f. Finally, the two-dimensional (2-D) time-frequency matrix ($\mathbf{GST}(k,n)$) of the discrete signal based on $h(t)$ is obtained by the GST as follows.

$$\mathrm{GST}(k,n) = A(k,n)\,e^{j\varphi(k,n)} \tag{13}$$

Here, $A(k,n)$ is the amplitude matrix and $\varphi(k,n)$ is the phase matrix. The rows of $A(k,n)$ and $\varphi(k,n)$ correspond to the amplitude and phase vary with the time at a certain sampled frequency point, respectively, and the columns of $A(k,n)$ and $\varphi(k,n)$ correspond to the amplitude and phase vary with the frequency at a certain sampled time point, respectively.

B. DENOISING METHOD

The proposed denoising method is schematically illustrated by the flow chart shown in Fig. 3. Here, threshold filtering and time-frequency distribution filtering are applied in sequence to $\mathbf{GST}(k,n)$, which is obtained by applying the discrete GST_σ to the discrete time series based on $h(t)$. Finally, the discrete denoised signal is obtained by applying the discrete inverse GST_σ. The denoising process is described as follows.

Firstly, threshold filtering is applied to $\mathbf{GST}(k,n)$ based on a determined threshold η. The appropriate value of η is obtained by first determining the overall range of $\mathbf{GST}(k,n)$, which is given as the difference between the maximum $\mathbf{GST}_H = \max(\mathbf{GST}(k,n))$ and the minimum $\mathbf{GST}_L = \min(\mathbf{GST}(k,n))$. Then, the overall range is divided into $K = 2^n$ (i.e., $n = 7, 8$) intervals as follows.

$$\Delta p = \frac{\mathrm{GST}_H - \mathrm{GST}_L}{K} \tag{14}$$

The range of each interval is

$$\delta = (\mathrm{GST}_L + \Delta p(K-1), \mathrm{GST}_L + \Delta p \cdot K). \tag{15}$$

Then, the appropriate value of η is obtained by analyzing data in each interval. The threshold function is given as follows.

$$H_1(k,n) = \begin{cases} 1, & \mathrm{GST}(k,n) \geq \eta \\ 0, & \mathrm{GST}(k,n) < \eta \end{cases} \quad (k,n) \in R \tag{16}$$

After conducting threshold filtering, $\mathbf{GST}(k,n)$ is transformed as follows.

$$\mathrm{GST}_1(k,n) = \mathrm{GST}(k,n) * H_1(k,n) \tag{17}$$

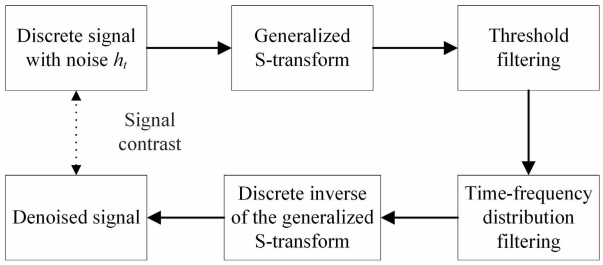

FIGURE 3. Flow chart illustrating the proposed denoising method.

Secondly, time-frequency distribution filtering is applied to $\mathbf{GST_1}(k, n)$. A noisy signal $h(t)$ can be described as the sum of an effective signal $x(t)$ and a noise signal $n(t)$, as follows.

$$h(t) = x(t) + n(t) \tag{18}$$

This relationship is preserved in the transformed version of $h(t)$ as follows.

$$\mathrm{GST}_h(k, n) = \mathrm{GST}_x(k, n) + \mathrm{GST}_n(k, n) \tag{19}$$

As a result, $\mathbf{GST_x}(k, n)$ can be obtained if $\mathbf{GST_n}(k, n) = 0$. As shown in Fig. 4, time-frequency distribution filtering eliminates $\mathbf{GST_n}(k, n)$ based on the clustering of $\mathbf{GST_x}(k, n)$ and $\mathbf{GST_n}(k, n)$ in the time-frequency domain. Therefore, the range of the noise signal time and frequency can be determined analyzing the time-frequency distribution of noisy signal. The time-frequency distribution function is then given as follows.

$$H_2(k, n) = \begin{cases} 1, & t \in [t_1, t_2] \,\&f \in [f_1, f_2] \\ 1, & t \in [t_3, t_4] \,\&f \in [f_3, f_4] \\ 1, & \vdots \\ 1, & t \in [t_{k-1}, t_k] \,\&f \in [f_{n-1}, f_n] \\ 0, & else \end{cases} \tag{20}$$

After conducting time-frequency distribution filtering, $\mathbf{GST_1}(k, n)$ is transformed as follows.

$$\mathrm{GST}_2(k, n) = \mathrm{GST}_1(k, n) * H_2(k, n) \tag{21}$$

Finally, applying the discrete inverse of the GST yields the effective signal as follows.

$$x(t) = \mathrm{GST}^{-1}[\mathrm{GST}_2(k, n)] \tag{22}$$

IV. COMPREHENSIVE MULTI-CRITERIA FAULTY FEEDER DETECTION METHOD

A. TRANSIENT ZERO-SEQUENCE CURRENT POLARITY CRITERION

As discussed above, the transient zero-sequence current of a faulty feeder has a polarity that is opposite to that of a healthy feeder in the SFB [30]. Therefore, a faulty feeder can be identified if its transient zero-sequence current has the opposite polarity from those of all other feeders. Moreover, the faulty feeder can be identified as the bus if these current polarities are equivalent for all feeders in the RG system. Therefore, for

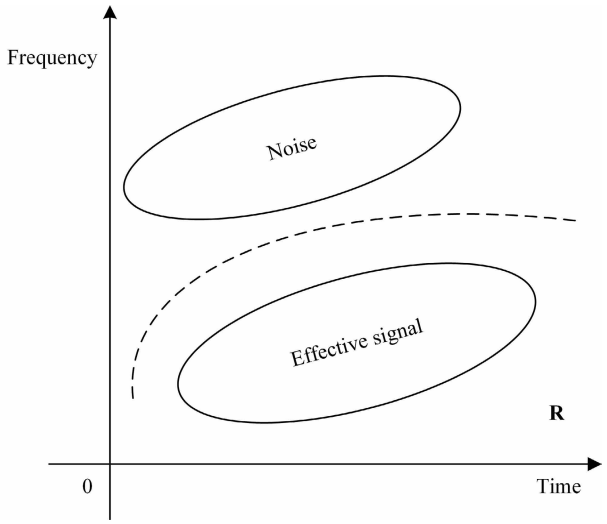

FIGURE 4. Time-frequency filtering based on time-frequency distributions.

an RG system composed of l feeders ($l \geq 2$), the transient zero-sequence current polarity criterion can be formulated according to the following polarity relation between feeder i and feeder j.

$$P_{ij} = \frac{1}{N} \sum_{t_k=0}^{N-1} i_{0i}(t_k)\, i_{0j}(t_k) \quad i, j = 1, 2, \ldots, l \; i \neq j \tag{23}$$

If $P_{ij} > 0$, then i_{0i} and i_{0j} have the same polarity, while, if $P_{ij} < 0$, i_{0i} and i_{0j} have the opposite polarity. For example, if $i = a$, $P_{aj} < 0\,(j \neq a)$, and all the other $i \neq a$, $P_{ij} > 0\,(j \neq i)$, then feeder a is the faulty feeder. In addition, if $P_{ij} > 0$ for all i and $j\,(j \neq i)$, then the bus is the faulty feeder.

B. TRANSIENT CURRENT ENERGY RELATIVE ENTROPY CRITERION

Relative entropy, also known as Kullback-Leibler divergence or information divergence, is used to measure the difference between two probability distributions. For example, the relative entropy between $P = \{P_1, P_2, \ldots, P_n\}$ and $Q = \{Q_1, Q_2, \ldots, Q_n\}$ is calculated as follows.

$$D_{KL}(P \parallel Q) = \sum_{x=1}^{n} \left\{ P_x \ln \frac{P_x}{Q_x} \right\} \tag{24}$$

Here, $D_{KL}(P \parallel Q) = 0$ when $P = Q$, and increases as the difference between the two probability distributions increases. This expression is then employed to evaluate the differences between the transient zero-sequence current energies of all feeders in the SFB. Firstly, the transient energy of feeder $i\,(i = 1, 2, \ldots, l, l \geq 2)$ at frequency f_n is defined as follows [16], [31].

$$E_{i\_n} = \sum_{k} [\mathrm{GST}_i(k, n)]^2 \tag{25}$$

The transient energy of all feeders at frequency f_n is then given as follows.

$$E_n = \sum_{i=1}^{l} E_{i\_n} = \sum_{i=1}^{l} \sum_{k} [\mathrm{GST}_i(k, n)]^2 \tag{26}$$

Then, the weight coefficient of feeder i at frequency f_n, which is defined as

$$p_{i\_n} = \frac{E_{i\_n}}{E_n}, \tag{27}$$

where $\sum_i p_{i\_n} = 1$, is employed in (24) to evaluate the differences between the transient energies of feeder i and feeder j as follows.

$$M_{ij} = \sum_{n} \left| p_{i\_n} \ln \frac{p_{i\_n}}{p_{j\_n}} \right| \tag{28}$$

Thus, the current energy relative entropy between feeder i and all other feeders is

$$M_i = \sum_{j=1, j\neq i}^{l} M_{ij}. \tag{29}$$

Clearly, the energy relative entropy between a faulty feeder and healthy feeders is greater than that between healthy feeders in the SFB because the amplitude of the transient current is larger for a faulty feeder than that of any healthy feeder. Therefore, as for a network with more than three feeders, the transient energy relative entropy criterion can be formulated by sorting the top three energy relative entropy values as M_a, M_b, and M_c (corresponding respectively to feeder a, feeder b, and feeder c) from top to bottom. If $M_a > M_b + M_c$, then feeder a is the faulty feeder. While the network with two feeders, the feeder a is the faulty feeder if $M_a > M_b$.

C. TOTAL TRANSIENT CURRENT ENERGY CRITERION

Based on (25), the transient zero-sequence current energy of feeder i ($i = 1, 2, \ldots, l, l \geq 3$) can be calculated over all frequencies as follows.

$$E_i = \sum_{n} \sum_{k} [\mathrm{GST}_i(k, n)]^2 \tag{30}$$

According to the law of energy conservation, the transient energy E_i produced by faulty feeder i is equivalent to the transient energy consumed by arc suppression coils E_L and all healthy feeders j in the SFB [32]. This relationship can be expressed as follows.

$$E_L + E_i + \sum_{j=1, j\neq i}^{l} E_j = 0 \tag{31}$$

To take advantage of this relationship, we define the difference between E_i and the sum of all other E_j as follows.

$$\Delta E_i = \left| |E_i| - \sum_{j=1, j\neq i}^{l} |E_j| \right| \tag{32}$$

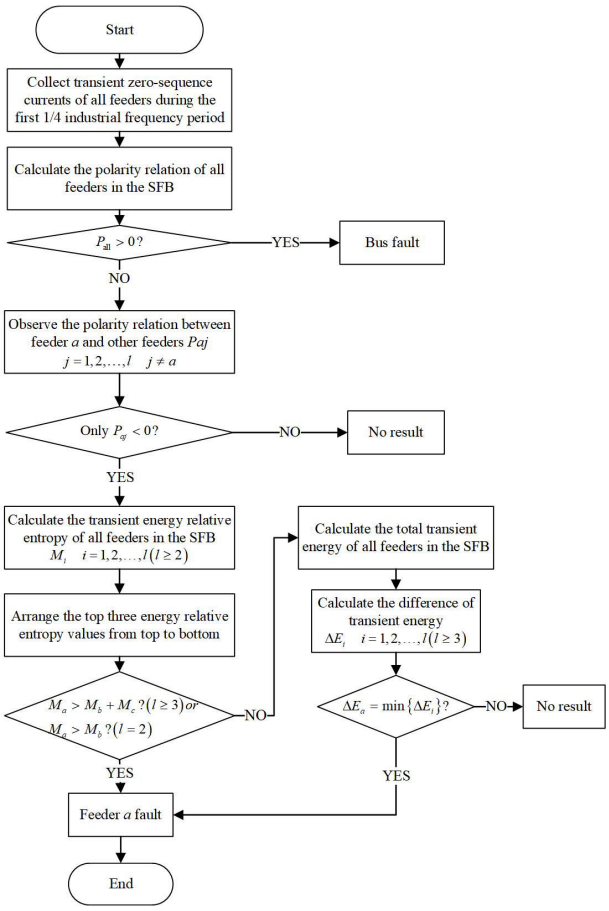

FIGURE 5. Flowchart of the proposed comprehensive multi-criteria faulty feeder detection method.

Consequently, the faulty feeder can be identified as the feeder i for which ΔE_i is smallest. This can be formalized as follows.

$$\Delta E_f = \min\{\Delta E_i\} \tag{33}$$

Therefore, the total transient energy criterion identifies the faulty feeder as the feeder i meeting the condition $\Delta E_i = \Delta E_f$.

D. MULTI-CRITERIA FAULTY FEEDER DETECTION PROCESS

The above three criteria were employed for detecting faulty feeders according to the process illustrated by the flow chart in Fig. 5. Firstly, the polarities of all feeders are assessed, and, if all feeders have the same polarity (i.e., $P_{\mathrm{all}} > 0$), the detection result is a bus fault, and the process terminates. Otherwise, detection accuracy is enhanced by applying both the current polarity criterion (criterion 1) and the transient energy relative entropy criterion (criterion 2) simultaneously to determine if feeder a is faulty, and accepting a positive decision only if the decisions of both criteria are positive. However, the process yields no detection result if the decision of criterion 1 is negative. Otherwise, the total transient energy criterion (criterion 3) is applied to determine if feeder a is faulty. If so, then a positive decision is obtained; otherwise, the process yields no detection result.

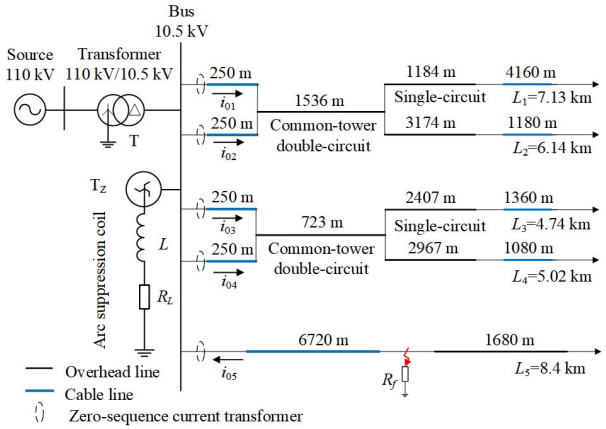

FIGURE 6. Model of 10 kV RG distribution network.

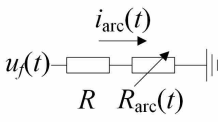

FIGURE 7. Arc discharge model.

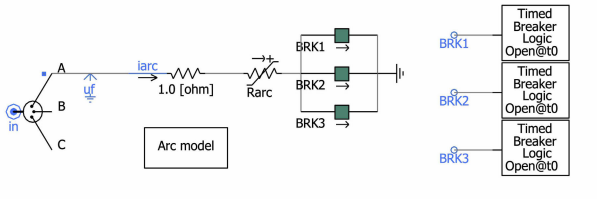

FIGURE 8. Arc discharge model established in PSCAD.

V. MODELS AND SIMULATIONS

A. 10 KV RG DISTRIBUTION NETWORK MODEL

A model of the 10 kV RG distribution network illustrated in Fig. 6 was established in PSCAD. This model is based on a section of an actual medium-voltage distribution network in Jiangsu Province, China. A frequency dependent (phase) model was adopted for establishing the line model in PSCAD because the line component characteristics are related to the system frequency [33]. The system frequency is 50 Hz. A typical overhead and cable mixed line structure was adopted, where the overhead line includes single-circuit transmission lines and common-tower double-circuit transmission lines. The model adopted the parameters of JKLYJ-240 transmission cable for the common-tower double-circuit transmission lines, which are 2.26 km long in total, while the parameters of JKLYJ-150 transmission cable were adopted for the single-circuit transmission lines, which are 9.73 km long in total. The overall length of the overhead line is 31.43 km. The underground cable was modeled as YJV22-3*400-400, YJV22-3*300-300, and YJV22-3*150-150 cable, which is 15.5 km long in total.

The network includes 5 feeders, which are given as $L_1 = 7.13$ km, $L_2 = 6.14$ km, $L_3 = 4.74$ km, $L_4 = 5.02$ km, and $L_5 = 8.4$ km. Also shown in Fig. 6 is that an SLG fault has occurred at feeder L_5. For a 10% overcompensation degree of the distribution network, the inductance L and resistance R_L of the arc suppression coil can be calculated as $L = 2.47$ H and $R_L = 23.28\ \Omega$, respectively. In addition, i_{01}, i_{02}, i_{03}, i_{04}, and i_{05} are the zero-sequence currents of feeders L_1, L_2, L_3, L_4, and L_5, respectively.

B. ARC DISCHARGE MODEL

A standard arc discharge model is regarded as a description of the dynamic relationship between arc voltage and current. In the present study, a number of arc models have been subjected to comparison [33]. Kilicay arc model based on arc energy balance theory and control theory has been widely used, which was found to reflect arc grounding faults more intuitively and accurately. According to this model, the change in the instantaneous conductance of the arc $g(t)$ with respect to t is derived as follows [34].

$$\frac{dg(t)}{dt} = \frac{1}{\tau}\left[G(t) - g(t)\right] \tag{34}$$

Here, τ is the time constant of arc discharge, and $G(t)$ is the static conductance of the arc. According to the standard relationship, $g(t)$ can be expressed according to the arc resistance $R_{arc}(t)$ as follows.

$$R_{arc}(t) = \frac{1}{g(t)} \tag{35}$$

In addition, $G(t)$ can be expressed as a function of the arc current $i_{arc}(t)$ and the static arc voltage $u_{st}(t)$ as follows.

$$G(t) = \frac{|i_{arc}(t)|}{u_{st}(t)} \tag{36}$$

Here, $u_{st}(t)$ is given as

$$u_{st}(t) = u_{arc} + r_{arc}\,|i_{arc}(t)|\,, \tag{37}$$

where $u_{arc}(t)$ and $r_{arc}(t)$ are the characteristic voltage and resistance of the arc, respectively. Consequently, the dynamic mathematical arc model is described as follows.

$$\frac{dg(t)}{dt} = \frac{1}{\tau}\left(\frac{|i_{arc}(t)|}{u_{arc} + r_{arc}\,|i_{arc}(t)|} - g(t)\right) \tag{38}$$

It is noted that τ, $u_{arc}(t)$, and $r_{arc}(t)$ are characteristic parameters of arc discharge, and are usually considered constants. The values adopted in this paper are $\tau = 0.0002$ s, $u_{arc}(t) = 1500$ V, and $r_{arc}(t) = 0.005\ \Omega$.

The arc discharge model illustrated in Fig. 7 with a constant resistance R in series with $R_{arc}(t)$ was employed in the present work owing to the characteristics of overhead and underground cable lines and the physical processes of line faults. The mathematical form of the model is

$$u_f(t) = i_{arc}(t)\,R + i_{arc}(t)\,R_{arc}(t)\,, \tag{39}$$

where $u_f(t)$ is the arc grounding fault voltage. The arc discharge model established in PSCAD is shown in Fig. 8.

The waveforms of $i_{arc}(t)$, $u_f(t)$ and $R_{arc}(t)$ obtained by arc ground fault simulations in PSCAD are shown in Fig. 9.

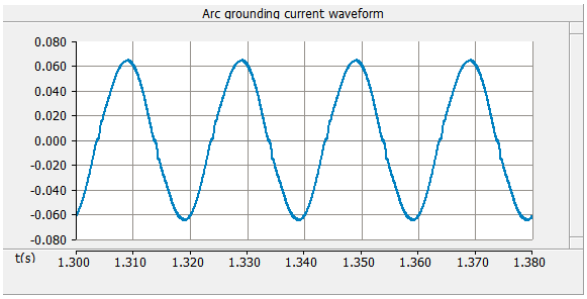

(a) Arc grounding current waveform.

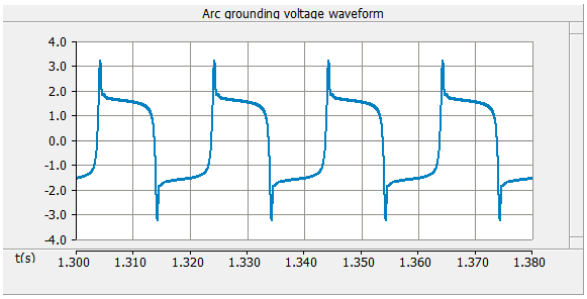

(b) Arc grounding voltage waveform.

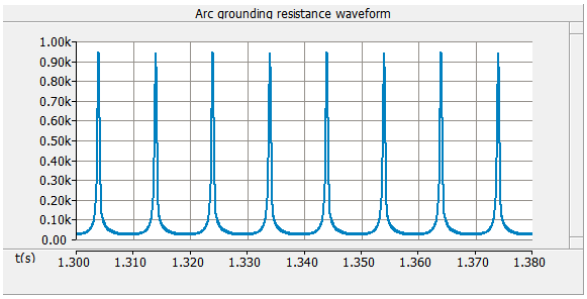

(c) Arc grounding resistance waveform.

FIGURE 9. Arc discharge waveforms of current, voltage, and resistance respectively obtained by arc grounding fault simulations based on the arc discharge model shown in Fig. 8.

C. DIFFERENT FAULT CONDITIONS TESTING

The performance of the proposed comprehensive multi-criteria faulty feeder detection method was evaluated for the modeled 10 kV RG distribution network under the constant resistance fault experiments with different fault conditions. It is verified from the aspects of different fault feeders, noise intensity, overcompensation degree, initial fault phase, fault resistance and fault distance, and specific fault conditions are shown in Table 2. Here, noisy environments with signal to noise ratio (SNR) values ranging from −10 dB to 10 dB were introduced in the simulations by adding white Gaussian noise with a zero mean and unit variance to the feeder signals according to the standard noisy signal model given in (18) using the awgn function of MATLAB.

In order to reflect the good performance of denoising method based on threshold filtering and time-frequency distribution filtering of GST with a variable factor proposed above, Fig. 10 shows the simulated transient zero-sequence current original waveforms, the current waveforms with added white Gaussian noise under low SNR (−5 dB) and

TABLE 2. Different fault conditions employed for testing the proposed faulty feeder detection method in the 10 kV RG system.

Faulty feeder	SNR (dB)	Overcompensation degree	Initial fault phase (°)	Fault resistance (Ω)	Fault distances (km)
L_1	-5	5%	0	10	1.27
	0	8%	45	300	1.82
	5	10%	90	1000	2.67
L_2	5	5%	30	100	2.06
	0	8%	60	500	1.61
	-5	10%	90	1000	1.97
L_3	-5	5%	0	10	1.5
	0	8%	45	300	1.9
	5	10%	90	1000	2.3
L_4	5	5%	30	100	2.2
	0	8%	60	500	2.7
	-5	10%	90	1000	1.55
L_5	-10	5%	0	10	1.77
	-5	5%	30	100	2.22
	0	8%	45	300	1.87
	5	8%	60	500	1.99
	10	10%	90	1000	2.47
Bus	-10	5%	0	10	—
	-5	5%	30	100	
	0	8%	45	300	
	5	8%	60	500	
	10	10%	90	1000	

denoised current waveforms of all feeders obtained during the first 1/4 industrial frequency period after a constant resistance SLG fault occurs in the feeder L_1, L_3, L_5, and bus respectively. The figures indicate that the denoising method has a perfect denoising effect even if the excessive noise nearly covers the signals. In addtion, the transient zero-sequence current polarity of faulty feeder is opposite to those of other feeders except that the current polarities of all feeders are equivalent when an SLG fault occurs in the bus.

Meanwhile, Fig. 11 presents the transient current energy relative entropy of all feeders in the SFB under −5 dB SNR condition after a constant resistance SLG fault occurs in the feeder L_1, L_3, L_5, and bus respectively. It indicates that the transient current energy relative entropy of faulty feeder significantly larger than that of any healthy feeder except when the fault occurs in the bus. However, the fault has already been detected in the bus by criterion 1 of the multi-criteria detection method. Therefore, the detection method can avoid misjudgment by comprehensive multi-criteria.

The detection results obtained during testing for all criteria are listed in Table 3. The detection results show that the criterion 2 has failed to detect the faulty feeder L_4, and the criterion 3 is applied to determine the faulty feeder. The results demonstrate that the proposed comprehensive multi-criteria detection method accurately detected the faulty feeder in all cases and indicate that the proposed detection method is robust against signal noise, overcompensation degree, initial fault phase, fault resistance, and fault location.

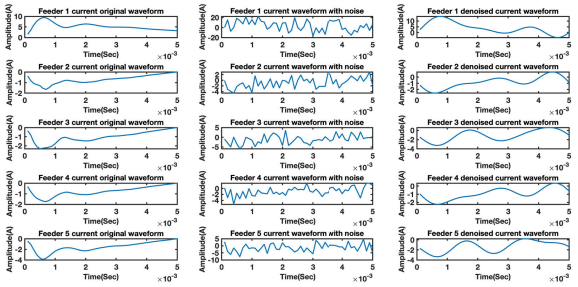

(a) An SLG fault occurs in the feeder L_1.

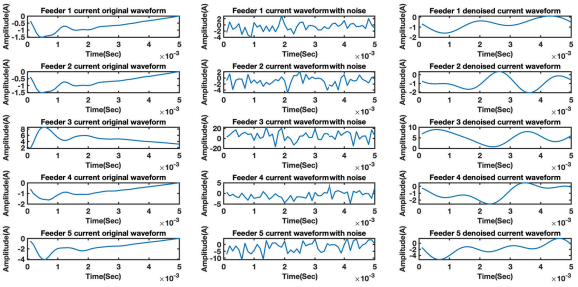

(b) An SLG fault occurs in the feeder L_3.

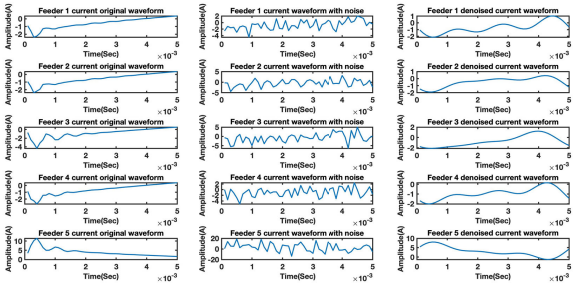

(c) An SLG fault occurs in the feeder L_5.

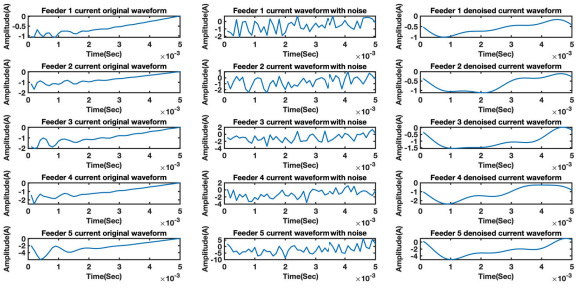

(d) An SLG fault occurs in the bus.

FIGURE 10. Three kinds of transient zero-sequence current waveforms of all feeders obtained during the first 1/4 industrial frequency period under −5 dB SNR condition after an SLG fault occurs in the feeder L_1, L_3, L_5, and bus respectively.

D. ARC GROUNDING FAULT TEST

Arc grounding faults are usually analyzed using high frequency theory and fundamental frequency theory [35]. While fundamental frequency theory provides analyses more proximate to practical networks, suggesting that arc discharges are immediately extinguished when discharge currents cross zero, actual arc grounding faults may last several cycles before extinguishing. Therefore, the accuracy and

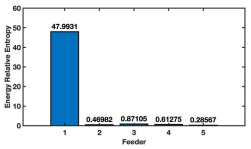

(a) An SLG fault occurs in the feeder L_1.

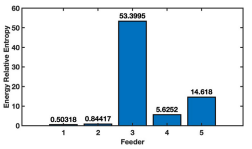

(b) An SLG fault occurs in the feeder L_3.

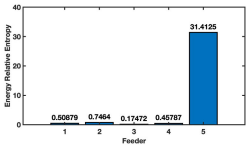

(c) An SLG fault occurs in the feeder L_5.

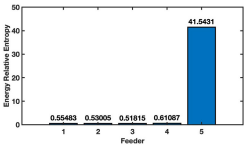

(d) An SLG fault occurs in the bus.

FIGURE 11. The transient current energy relative entropy of all feeders in the selected frequency band (SFB) under −5 dB SNR condition after an SLG fault occurs in the feeder L_1, L_3, L_5, and bus respectively.

TABLE 3. Detection results obtained under the different fault conditions listed in Table 2.

Faulty feeder	Criterion 1	Criterion 2	Criterion 3	Detection result
L_1	Only $P_{1j} < 0$	48.0>0.9+0.6	—	L_1
	Only $P_{1j} < 0$	47.7>1.7+1.3	—	
	Only $P_{1j} < 0$	40.4>0.7+0.6	—	
L_2	Only $P_{2j} < 0$	19.8>3.7+0.9	—	L_1
	Only $P_{2j} < 0$	19.5>3.8>2.1	—	
	Only $P_{2j} < 0$	45.2>5.6+2.4	—	
L_3	Only $P_{3j} < 0$	53.4>14.6+5.6	—	L_3
	Only $P_{3j} < 0$	39.9>5.0+0.4	—	
	Only $P_{3j} < 0$	25.3>4.3+1.0	—	
L_4	Only $P_{4j} < 0$	23.9>1.3+1.0	—	L_4
	Only $P_{4j} < 0$	17.0<23.6+2.5	ΔE_4	
	Only $P_{4j} < 0$	31.3>12.4+2.0	—	
L_5	Only $P_{5j} < 0$	60.0>0.7+0.5	—	L_5
	Only $P_{5j} < 0$	31.4>0.8+0.5	—	
	Only $P_{5j} < 0$	89.3>60.0+12.9	—	
	Only $P_{5j} < 0$	30.0>2.8+1.0	—	
	Only $P_{5j} < 0$	26.3>2.3+0.9	—	
Bus	$P_{\text{all}} > 0$	—	—	Bus
	$P_{\text{all}} > 0$	—	—	
	$P_{\text{all}} > 0$	—	—	
	$P_{\text{all}} > 0$	—	—	
	$P_{\text{all}} > 0$	—	—	

adaptability of the proposed comprehensive multi-criteria faulty feeder detection method were tested under the 22 kinds of permanent and intermittent arc grounding fault conditions listed in Table 4 with different faulty feeders, noise intensity, overcompensation degree, arc resumption intervals and fault distance. The permanent arc grounding fault is the arc grounding fault without arc resumption intervals and the intermittent arc grounding faults with 10 ms and 30 ms resumption intervals were simulated to resume and extinguish three times.

Fig. 12(a) and (b) present the transient zero-sequence currents obtained for all feeders in the 10 kV RG network during PSCAD simulations after a permanent arc grounding fault

TABLE 4. Different arc grounding fault conditions employed for testing the proposed faulty feeder detection method in the 10 kV RG system.

Faulty feeder	SNR (dB)	Overcompensation degree	Arc extinguishing and resumption intervals (ms)	Fault distances (km)
L_1	-5	5%	—	1.27
	0	8%	10	1.82
	5	10%	30	2.67
L_2	5	5%	—	2.06
	0	8%	10	1.61
	-5	10%	30	1.97
L_3	-5	5%	—	1.5
	0	8%	10	1.9
	5	10%	30	2.3
L_4	5	5%	—	2.2
	0	8%	10	2.7
	-5	10%	30	1.55
L_5	-10	5%	—	1.77
	-5	5%	10	2.22
	0	8%	10	1.87
	5	8%	30	1.99
	10	10%	30	2.47
Bus	-10	5%	—	—
	-5	5%	10	
	0	8%	10	
	5	8%	30	
	10	10%	30	

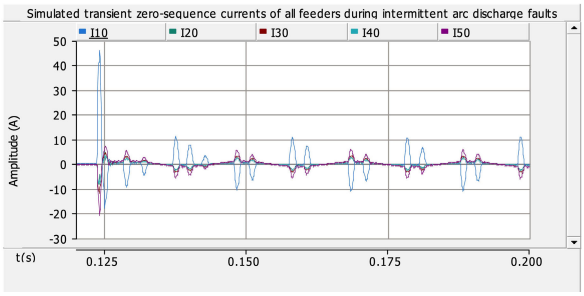

(a) A permanent arc grounding fault occurred in feeder L_1.

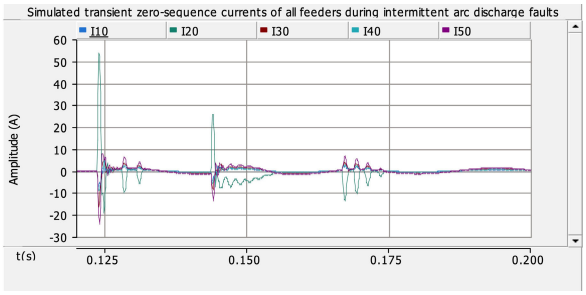

(b) An intermittent arc grounding fault with 10 ms resumption intervals occurred in feeder L_2.

FIGURE 12. Simulated zero-sequence currents of all feeders after arc grounding faults occurred in PSCAD.

occurs in the feeder L_1 and an intermittent arc grounding fault with the arc resumption intervals of 10 ms occurs in the feeder L_2.

Fig. 13 presents the comparisons of original current waveforms, current waveforms with noise, and denoised current waveforms of all feeders obtained during the first 1/4 industrial frequency period after an arc grounding fault occurs in the feeder L_1, L_2, L_3, and L_4 respectively, where (a) and (c) are current waveforms obtained after a permanent arc grounding fault occurs in the feeder L_1 and L_3 with an SNR of -5 dB respectively, (b) and (d) are current waveforms obtained after an intermittent arc grounding fault with 10 ms resumption intervals occurs in the feeder L_2 and L_4 with an SNR of 0 dB respectively. From these figures, we can see that the denoised waveforms have a little distortion

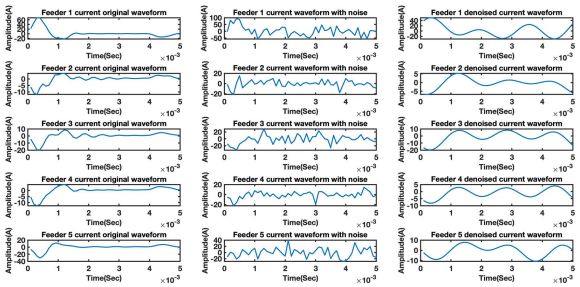

(a) A permanent arc grounding fault occurs in the feeder L_1.

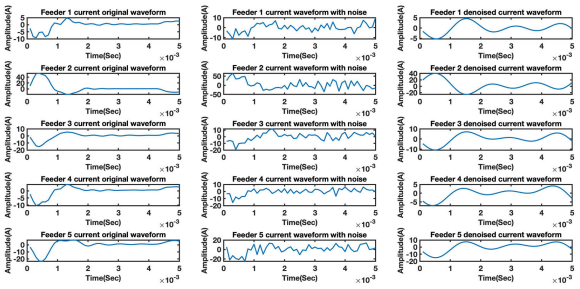

(b) An intermittent arc grounding fault with 10 ms resumption intervals occurs in the feeder L_2.

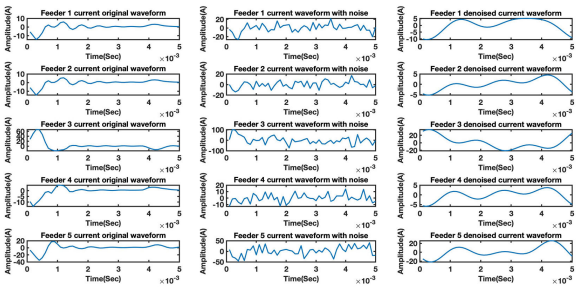

(c) A permanent arc grounding fault occurs in the feeder L_3.

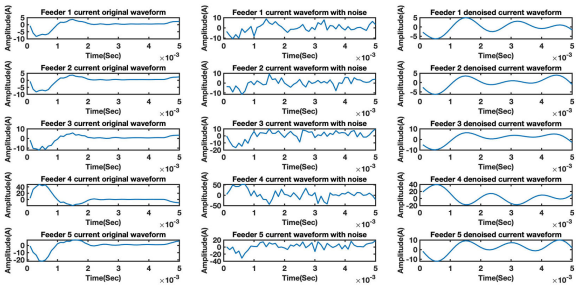

(d) An intermittent arc grounding fault with 10 ms resumption intervals occurs in the feeder L_4.

FIGURE 13. Three kinds of transient zero-sequence current waveforms of all feeders obtained during the first 1/4 industrial frequency period after an arc grounding fault occurs in the feeder L_1, L_2, L_3, and L_4 respectively.

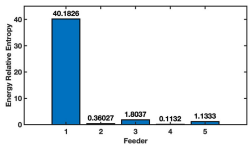

(a) A permanent arc grounding fault occurs in the feeder L_1.

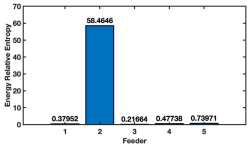

(b) An intermittent arc grounding fault with 10 ms resumption intervals occurs in the feeder L_2.

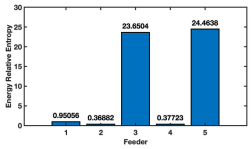

(c) A permanent arc grounding fault occurs in the feeder L_3.

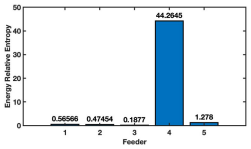

(d) An intermittent arc grounding fault with 10 ms resumption intervals occurs in the feeder L_4.

FIGURE 14. The transient current energy relative entropy of all feeders in the SFB after an arc grounding fault occurs in the feeder L_1, L_2, L_3, and L_4, and bus respectively.

under −5 dB SNR condition, but the multi-criteria detection method can still identify the correct faulty feeder. However, the transient zero-sequence currents can be denoised perfectly to recover the original signals from noisy signals corrupted by additive noise under 0 dB and above SNR conditions whether permanent or intermittent arc grounding faults occur.

Meanwhile, Fig. 14 presents the transient current energy relative entropy of all feeders in the SFB after an arc grounding fault occurs in the feeder L_1, L_2, L_3, and L_4 respectively. Fig. 14 shows that the criterion 2 has failed to detect the faulty feeder L_3, and the criterion 3 is applied to determine the faulty feeder. It is noted that arc grounding faults exhibit more obvious transient signal characteristics than constant resistance faults. Moreover, the respective conditions considered by criteria 1 and 2 are obviously apparent in Figs. 13 and 14.

The detection results obtained during testing for all criteria are listed in Table 5. The results demonstrate that the proposed faulty feeder detection method provides accurate detection under a wide range of arc grounding fault conditions.

VI. COMPARED WITH EXISTING METHODS

A. DENOISING EFFECT

Existing denoising methods include adaptive MM filtering, WT threshold filtering, and adaptive time-frequency filtering using the ST. Therefore, the performance of the proposed GST_σ-based denoising method was compared with the method without denoising and those of these three existing methods based on the SNR of the denoised signal and the mean squared error (MSE) between the denoised signal and the known effective signal.

$$\mathrm{SNR}= 10lg\left(\frac{\frac{1}{N}\sum_{n=1}^{N}s(n)^2}{\frac{1}{N}\sum_{n=1}^{N}\left(|x\,(n)|-|s\,(n)|\right)^2}\right) \tag{40}$$

TABLE 5. Detection results obtained under different arc grounding fault conditions listed in Table 4.

Faulty feeder	Criterion 1	Criterion 2	Criterion 3	Detection result
L_1	Only $P_{1j}<0$	40.2>1.8+1.1	—	L_1
	Only $P_{1j}<0$	48.9>1.4+0.4	—	
	Only $P_{1j}<0$	39.5>1.3+0.5	—	
L_2	Only $P_{2j}<0$	46.2>1.5+0.6	—	L_1
	Only $P_{2j}<0$	58.5>0.7+0.5	—	
	Only $P_{2j}<0$	60.2>0.8+0.4	—	
L_3	Only $P_{3j}<0$	23.7<24.5+1.0	ΔE_3	L_3
	Only $P_{3j}<0$	41.9>2.4+0.4	—	
	Only $P_{3j}<0$	42.2>1.1+0.5	—	
L_4	Only $P_{4j}<0$	38.3>1.2+0.5	—	L_4
	Only $P_{4j}<0$	44.3>1.3+0.6	—	
	Only $P_{4j}<0$	43.7>6.5+0.9	—	
L_5	Only $P_{5j}<0$	55.4>2.0+1.0	—	L_5
	Only $P_{5j}<0$	54.5>0.4+0.3	—	
	Only $P_{5j}<0$	60.3>0.4+0.3	—	
	Only $P_{5j}<0$	54.2>0.5+0.5	—	
	Only $P_{5j}<0$	46.6>0.5+0.5	—	
Bus	$P_{\mathrm{all}}>0$	—	—	Bus
	$P_{\mathrm{all}}>0$	—	—	
	$P_{\mathrm{all}}>0$	—	—	
	$P_{\mathrm{all}}>0$	—	—	
	$P_{\mathrm{all}}>0$	—	—	

$$\mathrm{MSE}=\frac{1}{N}\sum_{n=1}^{N}\left(|x\,(n)|-|s\,(n)|\right)^2 \tag{41}$$

Here, N is the number of sampling points, $x\,(n)$ is the denoised signal and $s\,(n)$ is the origin signal without noise. It can be seen that the denoising performance increases as the post-filtering SNR value increases and as the MSE decreases. As was conducted previously, white Gaussian noise was added to simulate noisy environments with SNR values ranging from −10 dB to 10 dB.

The denoising performance of the simulated signals obtained for feeder L_1 are listed in Table 6 under different constant resistance faults and arc grounding faults occurring in feeder L_1 of the 10 kV RG system. The effective, noisy, and denoised current waveforms of L_1 are also presented in Fig. 15 under constant resistance faults and arc grounding faults with different SNR conditions. We note from Table 6 that the denoising performance of the proposed GST_σ filtering is substantially greater than those of MM adaptive filtering and ST adaptive filtering below 0 dB SNR condition for both constant resistance faults and arc grounding faults. We also note that the differences between the denoising performances of WT filtering and GST_σ filtering are not substantial above 0 dB SNR condition, particularly when the noise is very small relative to the effective signal at SNR values of 5 dB and 10 dB. However, a subjective appraisal of Fig. 15 indicates that the waveform denoised by GST_σ filtering appears to be much closer to the waveform of the transient zero-sequence current of L_1 without noise than the waveforms denoised by other three methods. As such, we can

TABLE 6. Denoising performance results of the simulated signals obtained for L_1 during L_1 faults in the 10 kV RG system.

Fault type	Denoising method	-10 dB		-5 dB		0 dB		0 dB		10 dB	
		MSE	SNR	MSE	SNR	MSE	SNR	MSE	SNR	MSE	SNR
300 Ω resistance fault	-	108.19	-8.76	30.07	-3.20	11.86	0.84	3.56	6.07	1.56	9.64
	MM filtering	210.28	-11.64	18.36	-1.05	5.77	3.97	2.76	7.18	3.77	5.82
	WT filtering	28.70	-2.99	6.59	3.40	4.23	5.32	2.54	7.54	1.27	10.55
	ST filtering	12.19	0.73	13.00	0.45	12.29	0.69	11.82	0.86	12.01	10.79
	GST_σ filtering	**7.85**	**2.64**	**4.98**	**4.61**	**3.43**	**6.23**	**1.11**	**11.13**	**0.63**	**13.59**
1000 Ω resistance fault	-	17.00	-9.30	4.59	-3.62	1.49	1.28	0.50	5.99	0.19	10.16
	MM filtering	24.54	-10.89	7.62	-5.81	1.20	2.20	0.29	8.37	0.45	6.45
	WT filtering	3.08	-1.89	1.41	1.50	0.65	4.88	0.41	6.83	0.20	10.08
	ST filtering	1.51	1.22	1.08	2.69	1.08	2.69	1.16	2.37	1.08	2.65
	GST_σ filtering	**0.74**	**4.29**	**0.50**	**5.97**	**0.46**	**6.34**	**0.25**	**8.96**	**0.16**	**11.02**
Permanent arc grounding fault	-	3039.60	-9.09	1191.64	-5.02	356.90	0.21	127.22	4.69	25.26	11.71
	MM filtering	4330.30	-10.63	2647.83	-8.49	567.42	-1.80	196.62	2.80	115.59	5.11
	WT filtering	873.68	-3.67	212.73	2.46	109.41	5.35	104.44	5.55	27.65	10.84
	ST filtering	374.90	0.00	374.89	0.00	372.99	0.02	373.31	0.02	372.78	0.02
	GST_σ filtering	**276.06**	**1.33**	**121.51**	**4.89**	**104.55**	**5.55**	**54.86**	**8.35**	**19.55**	**12.83**
Intermittent arc grounding fault with 10 ms intervals	-	1748.08	-8.23	600.41	-3.59	233.06	0.52	80.38	5.14	26.85	9.91
	MM filtering	3276.15	-10.96	817.53	-4.93	253.87	0.15	107.09	3.90	78.42	5.25
	WT filtering	334.37	-1.05	157.12	2.23	71.74	5.64	33.61	8.93	**18.55**	**11.51**
	ST filtering	262.78	0.00	262.21	0.01	261.50	0.02	261.32	0.02	258.87	0.07
	GST_σ filtering	**253.21**	**0.16**	**66.83**	**5.95**	**53.67**	**6.90**	**28.34**	**9.67**	26.22	10.01

TABLE 7. The comparisons between paper [16], [31], [36] and this paper.

Method	Fault type	Faulty feeder	Initial fault phase (°)	SNR (dB)	Criterion 1	Criterion 2	Criterion 3	Result	Accuracy
Paper [16]	1000 Ω resistance fault	L_1	90	-10	—	62.86>0.14+0.74	—	L_1	Right
	Arc grounding fault	Bus	90	-5	—	33.79>7.74+3.99	—	L_5	Wrong
Paper [31]	1000 Ω resistance fault	L_1	90	-10	—	—	18.60<3.08+16.87	Bus	Wrong
	Arc grounding fault	Bus	90	-5	—	—	938.90<690.50+363.90	Bus	Right
Paper [36]	1000 Ω resistance fault	L_1	90	-10	—	5.45<2.92+2.61	—	Bus	Wrong
	Arc grounding fault	Bus	90	-5	—	38.13>18.31+17.12	—	L_1	Wrong
This paper	1000 Ω resistance fault	L_1	90	-10	$P_{1j} < 0$	39.02>1.03+10.75	—	L_1	Right
	Arc grounding fault	Bus	90	-5	$P_{\text{all}} > 0$	—	—	Bus	Right

TABLE 8. The comparison of calculation times.

Method	Calculation times/s
Paper [16]	0.087
Paper [26]	0.096
Paper [31]	0.0792
Paper [32]	0.060
Paper [36]	0.064
This paper	**0.05856**

TABLE 9. Detection results of field test.

Fault type	Criterion 1	Criterion 2	Criterion 3	Detection result
Metal grounding	$P_{114j} < 0$	420.2>5.0+3.3	—	No. 114
200 Ω resistance grounding	$P_{114j} < 0$	220.6>19.1+12.4	—	No. 114
500 Ω resistance grounding	$P_{114j} < 0$	126.5>6.8+4.8	—	No. 114
1000 Ω resistance grounding	$P_{114j} < 0$	184.5>12.8+11.3	—	No. 114
Arc grounding	$P_{114j} < 0$	236.4>4.3+4.0	—	No. 114

conclude that the denoising performance of the proposed method is better than the other methods considered.

B. DETECTION ACCURACY EVALUATION AND CALCULATION TIME

The detection accuracy of the proposed comprehensive multi-criteria faulty feeder detection method was evaluated by comparisons between the detection accuracies obtained for the modeled 10 kV RG system by the proposed method and those of existing methods [16], [32], [36] that uniformly rely on a single criterion, which are criterion 2 based on the GST, criterion 3 based on the ST, and criterion 2 based on the WT, respectively. The results are presented in Table 7. From the table, it can be seen the single-criterion detection methods are prone to misjudgment when the noise is very large relative to the effective signal or when an arc grounding fault occurs.

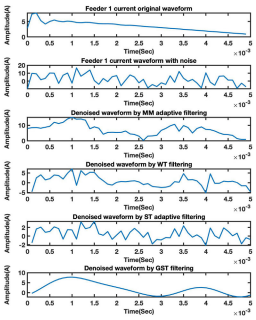

(a) 300 Ω resistance fault under -5 dB SNR condition.

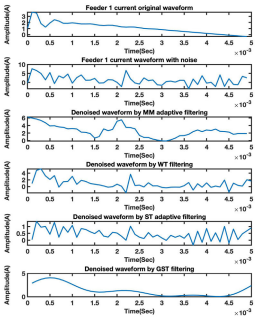

(b) 1000 Ω resistance fault under -5 dB SNR condition.

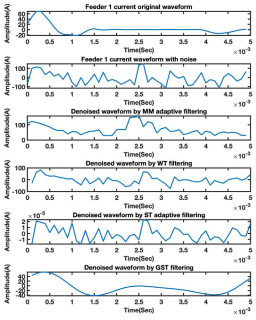

(c) Permanent arc grounding fault under -10 dB SNR condition.

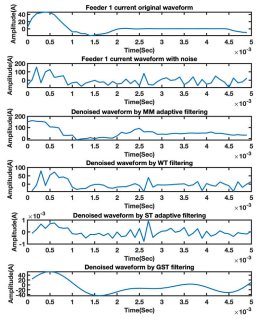

(d) Intermittent arc grounding fault with 10 ms intervals under -10 dB SNR condition.

FIGURE 15. Original, noisy, and denoised L_1 current waveforms obtained by four denoising methods under four different fault conditions.

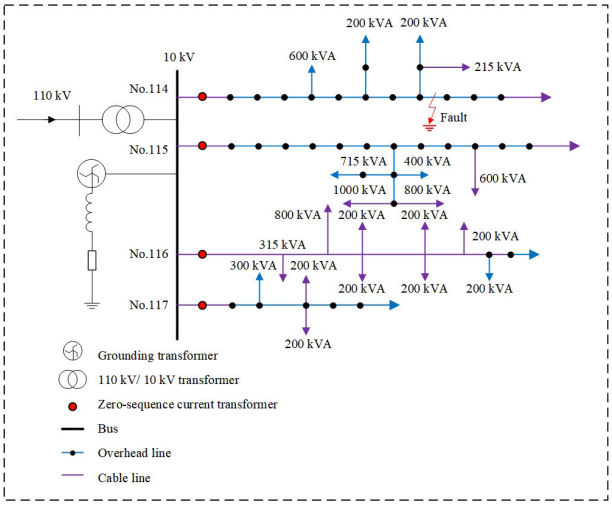

FIGURE 16. The 10 kV RG distribution network topology.

(a) Feeder terminal unit (FTU) added in the overhead line.

(b) SLG fault location test platform of distribution network.

(c) The scene of arc grounding fault occurrence in the controlled arc discharge device.

FIGURE 17. The scene when the SLG fault occurs in feeder No.114.

These results indicate that the method proposed in this paper provides superior faulty feeder detection accuracy than the existing methods considered.

In addition, the calculation times required by the compared detection methods were evaluated for the detection process results discussed above for the SLG fault, and the times are listed in Table 8. Here, the methods of paper [26] and paper [31] are added to test the compared calculation times. Paper [26] applied the single-criterion method based on the difference of two-phase current with SVM, and the method of paper [31] also applied single criterion based on ST energy from short window data. We note from the table that the proposed comprehensive multi-criteria detection method requires less calculation time than the other methods, particularly that of paper [26]. Therefore, in practical applications, the proposed method has a faster judgment speed.

VII. FIELD TEST OF SLG FAULT

In order to verify the performance of the proposed method, we carried out a field test at 10 kV distribution power line

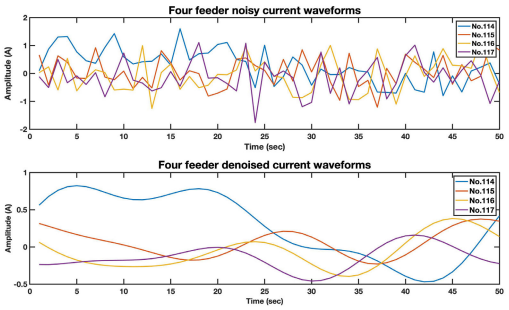

FIGURE 18. **Four feeders noisy and denoised zero-sequence current waveforms obtained after the SLG fault occurred in feeder No.114.**

of Jiangsu in China. The 10 kV RG distribution network topology is shown in Fig. 16, of which the main transformer is 110 kV/10 kV by an arc suppression coil grounding to land. We chose four feeders on the bus as the test lines, which are named No. 114, No. 115, No. 116, and No. 117. In addition, the overcompensation degree of this test system is 17.63% and the capacitive current is 47.26 A. In this field test, five kinds of SLG faults have been set in feeder No.114, which contain metal grounding fault, 200 Ω resistance grounding fault, 500 Ω resistance grounding fault, 1000 Ω resistance grounding fault, and arc grounding fault.

Fig. 17 shows the scene when the SLG fault occurs in feeder No.114, where (a) shows the feeder terminal unit (FTU) added in the overhead line to construct test branch, (b) shows the SLG fault location test platform of distribution network, and (c) shows the scene of arc grounding fault occurrence in the controlled arc discharge device. Moreover, Fig. 18 displays the collected zero-sequence current waveforms of four feeders after the SLG fault occurred in the feeder No.114, which belongs to 1000 Ω resistance fault under the noisy environment. From the figure, we observe that the transient fault characteristics covered by noise can be extracted clearly.

Meanwhile, the faulty feeder detection results by multi-criteria are listed in Table 9, which can be seen that the detection results are all correct. Therefore, it is verified that the proposed multi-criteria faulty feeder detection method can also produce accurate judgment results in the actual 10 kV RG distribution network.

VIII. CONCLUSION

This paper addressed the issues surrounding the detection of faulty feeders in RG power distribution networks by proposing a modified GST with a variable factor for self-adaptively adjusting the local window resolution of the time-frequency spectrum, and then applied the time-frequency representation of the GST to conduct denoising of transient zero-sequence currents based on threshold filtering followed by time-frequency distribution filtering in sequence. In addition, a comprehensive multi-criteria faulty feeder detection method was proposed. The results obtained by both a large number of simulation experiments and field test under different constant resistance faults and arc grounding faults have demonstrated the following conclusions.

(i) The GST provides a powerful time-frequency analysis proficiency compared with those of the ST and WT. The introduction of a variable factor into the GST has greatly improved its self-adaptability. As a result, the sequence of threshold filtering and time-frequency distribution filtering based on the time-frequency representation of the modified GST provides superior denoising performance compared to existing methods. Therefore, the detection method can identify faulty feeders accurately even in extremely noisy environments.

(ii) The proposed comprehensive multi-criteria detection method considers both the direction of transient zero-sequence signals (criterion 1) as well as the transient current energies of the feeders using two criteria based on the time-frequency representation of the modified GST (i.e., the current energy relative entropy [criterion 2] and the total current energy [criterion 3]), which provides faulty feeder detection that is robust to widely varying fault conditions, including constant resistance faults and arc grounding fault conditions. The proposed detection method was demonstrated to provide higher faulty feeder detection accuracy and reduce calculation time compared to existing methods.

(iii) The modeled 10 kV RG distribution network with an overhead and cable mixed line structure and arc discharge fault model established in this paper ensured that the simulations faithfully represented actual complex working conditions. The detection results of field test can verify the reality and effectiveness of models and simulations established in this paper. Therefore, the simulation testing conducted in this paper can be expected to provide realistic results.

REFERENCES

[1] *Technical Guidelines for Distribution Network*, Standard Q/GDW 10370, 2016.

[2] Y. Xiao, J. Ouyang, X. Xiong, Y. Wang, and Y. Luo, "Fault protection method of single-phase break for distribution network considering the influence of neutral grounding modes," *Protection Control Mod. Power Syst.*, vol. 5, no. 1, pp. 111–123, Dec. 2020.

[3] S. K. Mishra and L. N. Tripathy, "A critical fault detection analysis & fault time in a UPFC transmission line," *Protection Control Mod. Power Syst.*, vol. 4, no. 1, pp. 24–33, Dec. 2019.

[4] W. Fan and Y. Liao, "Wide area measurements based fault detection and location method for transmission lines," *Protection Control Mod. Power Syst.*, vol. 4, no. 1, pp. 53–64, Dec. 2019.

[5] T. Jain, D. Ghosh, and D. K. Mohanta, "Augmentation of situational awareness by fault passage indicators in distribution network incorporating network reconfiguration," *Protection Control Mod. Power Syst.*, vol. 4, no. 4, pp. 323–336, 2019.

[6] M. T. Hagh, H. Rezaei, and M. Daneshvar, "Faulted feeder identification in active grounded networks," *IET Gener., Transmiss. Distrib.*, vol. 13, no. 15, pp. 3476–3483, Aug. 2019.

[7] X. Wang, G. Song, Z. Chang, J. Luo, J. Gao, X. Wei, and Y. Wei, "Faulty feeder detection based on mixed atom dictionary and energy spectrum energy for distribution network," *IET Gener., Transmiss. Distrib.*, vol. 12, no. 3, pp. 596–606, Feb. 2018.

[8] F. Guo, H. Gao, Z. Wang, J. You, A. Tang, and Y. Zhang, "Detection and line selection of series arc fault in multi-load circuit," *IEEE Trans. Plasma Sci.*, vol. 47, no. 11, pp. 5089–5098, Nov. 2019.

[9] M.-F. Guo, X.-D. Zeng, D.-Y. Chen, and N.-C. Yang, "Deep-learning-based earth fault detection using continuous wavelet transform and convolutional neural network in resonant grounding distribution systems," *IEEE Sensors J.*, vol. 18, no. 3, pp. 1291–1300, Feb. 2018.
[10] B. Patel and P. Bera, "Fast fault detection during power swing on a hybrid transmission line using WPT," *IET Gener., Transmiss. Distrib.*, vol. 13, no. 10, pp. 1811–1820, May 2019.
[11] C. Chen, F. Guo, Y. Liu, Z. Wang, Y. Chen, and H. Liang, "Recognition of series arc fault based on the Hilbert huang transform," in *Proc. IEEE 61st Holm Conf. Electr. Contacts (Holm)*, Oct. 2015, pp. 324–330.
[12] X. Wang, J. Gao, X. Wei, Z. Zeng, Y. Wei, and M. Kheshti, "Single line to ground fault detection in a non-effectively grounded distribution network," *IEEE Trans. Power Del.*, vol. 33, no. 6, pp. 3173–3186, Dec. 2018.
[13] R. G. Stockwell, L. Mansinha, and R. P. Lowe, "Localization of the complex spectrum: The s transform," *IEEE Trans. Signal Process.*, vol. 44, no. 4, pp. 998–1001, Apr. 1996.
[14] C. R. Pinnegar and L. Mansinha, "The *S*-transform with windows of arbitrary and varying shape," *Geophysics*, vol. 68, no. 1, pp. 381–385, Jan. 2003.
[15] Z. Zhou and Y. Chen, "Generalized *S*-transform with variable-factor and its time-frequency filtering," *Coal Geol. Explor.*, vol. 39, no. 6, pp. 63–66, and 71, 2011.
[16] L. He, C. Shi, Z. Yan, J. Cui, and B. Zhang, "A fault section location method for small current neutral grounding system based on energy relative entropy of generalized S-transform," *Trans. China Electrotech. Soc.*, vol. 32, no. 8, pp. 274–280, 2017.
[17] M. Shafiullah and M. A. Abido, "S-transform based FFNN approach for distribution grids fault detection and classification," *IEEE Access*, vol. 6, pp. 8080–8088, 2018.
[18] N. Peng, K. Ye, R. Liang, T. Hou, G. Wang, X. Chen, and S. Teng, "Single-phase-to-earth faulty feeder detection in power distribution network based on amplitude ratio of zero-mode transients," *IEEE Access*, vol. 7, pp. 117678–117691, 2019.
[19] B. Gou and K. O. Owusu, "Linear relation between fault location and the damping coefficient in faulted signals," *IEEE Trans. Power Del.*, vol. 23, no. 4, pp. 2626–2627, Oct. 2008.
[20] M. Liu, "A new correlation analysis approach to fault line selection based on transient main-frequency components," *Power Syst. Protection Control*, vol. 44, no. 2, pp. 74–79, 2016.
[21] M. A. Barik, A. Gargoom, M. A. Mahmud, M. E. Haque, H. Al-Khalidi, and A. M. T. Oo, "A decentralized fault detection technique for detecting single phase to ground faults in power distribution systems with resonant grounding," *IEEE Trans. Power Del.*, vol. 33, no. 5, pp. 2462–2473, Oct. 2018.
[22] H. Shu, H. Huang, X. Tian, J. Dong, and R. Huang, "Fault line selection in resonant Earthed system based on morphological peak-valley detection," *Autom. Electr. Power Syst.*, vol. 43, no. 1, pp. 228–233, 2019.
[23] R. Godse and S. Bhat, "Mathematical morphology-based feature-extraction technique for detection and classification of faults on power transmission line," *IEEE Access*, vol. 8, pp. 38459–38471, 2020.
[24] M.-F. Guo and N.-C. Yang, "Features-clustering-based Earth fault detection using singular-value decomposition and fuzzy c-means in resonant grounding distribution systems," *Int. J. Electr. Power Energy Syst.*, vol. 93, pp. 97–108, Dec. 2017.
[25] X. Shao, M. Guo, and L. You, "Faulty line selection method using mutual correlation cluster of grounding fault waveforms based on improved DTW method," *Electr. Power Autom. Equip.*, vol. 38, no. 11, pp. 63–71, and 78, 2018.
[26] K. Chen and B. Chen, "Research on arc fault line selection based on improved transient correlation analysis and support vector machine," *Power Syst. Protection Control*, vol. 44, no. 24, pp. 66–73, 2016.
[27] B. K. Chaitanya, A. Yadav, and M. Pazoki, "An intelligent detection of high-impedance faults for distribution lines integrated with distributed generators," *IEEE Syst. J.*, vol. 14, no. 1, pp. 870–879, Mar. 2020.
[28] J. Cai and X. Li, "Gear fault diagnosis based on time–frequency domain de-noising using the generalized s transform," *J. Vib. Control*, vol. 24, no. 15, pp. 3338–3347, Aug. 2018.
[29] S. V. Khond and G. A. Dhomane, "Optimum coordination of directional overcurrent relays for combined overhead/cable distribution system with linear programming technique," *Protection Control Mod. Power Syst.*, vol. 4, no. 1, pp. 114–120, Dec. 2019.
[30] Y. Xue, Z. Feng, and B. Xu, "Analysis of transient characteristics of signals phase earth fault in non-solidly Earthed network," *J. Xi'an Jiaotong Univ.*, vol. 38, no. 2, pp. 195–199, 2004.
[31] H. Shu and S. Peng, "A fault line detection algorithm for distribution network of overhead line and underground cable mixed lines using S-transform energy from short window data," *Trans. China Electrotechn. Soc.*, vol. 24, no. 10, pp. 152–159, 2009.
[32] H. Shu and J. Liu, "Adaptive method for fault circuit selection in arc suppression coils system by using transient energy," *Autom. Electr. Power Syst.*, vol. 30, no. 11, pp. 72–76, 2006.
[33] L. Wang, H. Gao, and G. Zou, "Modeling methodology and fault simulation of distribution networks integrated with inverter-based DG," *Protection Control Mod. Power Syst.*, vol. 2, no. 1, pp. 370–378, Dec. 2017.
[34] Y. Xu, M. Guo, B. Chen, and G. Yang, "Modeling and simulation analysis of arc in distribution network," *Power Syst. Protection Control*, vol. 43, no. 7, pp. 57–64, 2015.
[35] R. Gu, X. Cai, H. Chen, Z. Jin, and W. Gao, "Modeling and simulating of single-phase arc grounding fault in non-effective Earthed networks," *Autom. Electr. Power Syst.*, vol. 33, no. 13, pp. 63–67, 2009.
[36] H. Shu and S. Peng, "Distribution network fault line detection using the full waveband complex relative entropy of wavelet energy," *High Voltage Eng.*, vol. 35, no. 7, pp. 1559–1564, Jul. 2009.

ZHINONG WEI (Member, IEEE) received the B.S. degree from the Hefei University of Technology, Hefei, China, in 1984, the M.S. degree from Southeast University, Nanjing, China, in 1987, and the Ph.D. degree from Hohai University, Nanjing, in 2004.

He is currently a Professor of electrical engineering with the College of Energy and Electrical Engineering, Hohai University. His research interests include power system state estimation, integrated energy systems, smart distribution systems, optimization and planning, load forecasting, and integration of distributed generation into electric power systems.

YUEXUAN MAO received the B.S. degree in electrical engineering from the College of Energy and Electrical Engineering, Hohai University, Nanjing, China, in 2018, where she is currently pursuing the M.S. degree.

Her research interest includes the fault location for distribution networks.

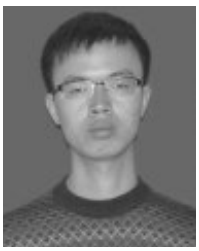

ZHIHUA YIN received the B.S. degree in electrical engineering from the China University of Mining and Technology, Xuzhou, China, in 2014, and the M.S. degree from Hohai University, Nanjing, China, in 2018, where he is currently pursuing the Ph.D. degree.

His research interest includes the fault location for distribution networks.

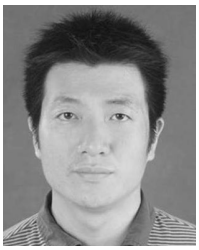

GUOQIANG SUN received the B.S., M.S., and Ph.D. degrees in electrical engineering from Hohai University, Nanjing, China, in 2001, 2005, and 2010, respectively.

From 2015 to 2016, he was a Visiting Scholar with North Carolina State University, Raleigh, NC, USA. He is currently an Associate Professor with the College of Energy and Electrical Engineering, Hohai University. His research interests include power system analysis, economic dispatch, and optimal control of integrated energy systems.

HAIXIANG ZANG received the B.S. degree in electrical engineering from Nanjing Normal University, in 2009, and the Ph.D. degree in electrical engineering from Southeast University, in 2014.

He is currently an Associate Professor with the College of Energy and Electrical Engineering, Hohai University, Nanjing, China. His research interests include generation of renewable energy, operation, and control of power systems, and so on.